WILEY-VCH

DOI: 10.1002/((solr.201800113a))
Article type: Communication

A High Efficiency Si Photoanode Protected by Few-Layer $MoSe_2$

*Srinivas Vanka, Yongjie Wang, Pegah Ghamari, Sheng Chu, Ayush Pandey, Pallab Bhattacharya, Ishiang Shih, and Zetian Mi**

S. Vanka, Y. Wang, A. Pandey, Prof. P. Bhattacharya and Prof. Z. Mi
Department of Electrical Engineering and Computer Science, University of Michigan, Ann Arbor, 1301 Beal Avenue, Ann Arbor, MI 48109, USA

S. Vanka, Dr. S. Chu, P. Ghamari, Prof. I. Shih and Prof. Z. Mi
Department of Electrical and Computer Engineering, McGill University, 3480 University Street, Montreal, Quebec H3A 0E9, Canada

E-mail: ztmi@umich.edu

Keywords: transitional metal dichalcogenide, two-dimensional material, water splitting, photoelectrode, hydrogen, solar cell

Abstract

To date, the performance of semiconductor photoanodes has been severely limited by oxidation and photocorrosion. Here, we report on the use of earth-abundant $MoSe_2$ as a surface protection layer for Si-based photoanodes. Large area $MoSe_2$ film was grown on p^+-n Si substrate by molecular beam epitaxy. It is observed that the incorporation few-layer (~3 nm) epitaxial $MoSe_2$ can significantly enhance the performance and stability of Si photoanode. The resulting $MoSe_2$/p^+-n Si photoanode produces a light-limited current density of 30 mA/cm^2 in 1M HBr under AM 1.5G one sun illumination, with a current-onset potential of 0.3 V *vs* reversible hydrogen electrode (RHE). The applied bias photon-to-current efficiency (ABPE) reaches up to 13.8%, compared to the negligible ABPE values (< 0.1%) for a bare Si photoanode under otherwise identical experimental conditions. The photoanode further produced stable voltage of ~0.38 V *vs* RHE at a photocurrent density of ~2 mA/cm^2 for ~14 hrs under AM 1.5G one sun illumination. This work shows the extraordinary potential of two-dimensional transitional metal dichalcogenides in photoelectrochemical application and will contribute to the development of low cost, high efficiency, and highly stable Si-based photoelectrodes for solar hydrogen production.

The ever-increasing demand for energy has inspired intensive research on the development of sustainable and renewable energy sources to diminish our dependence on fossil fuels.[1] PEC water splitting is one of the most promising methods to convert solar energy into storable chemical energy in the form of H_2 production,[2] which is a clean and eco-friendly alternative fuel that can be stored, distributed and consumed on demand.[3] A PEC device generally consists of a semiconductor photocathode and photoanode, which collect photo-generated electrons and holes to drive H_2 and O_2 evolution reaction, respectively.[4] For practical application, it is essential that the semiconductor photoelectrodes can efficiently harvest sunlight, are of low cost, and possess a high level of stability in aqueous solution. To date, however, it has remained challenging, especially for semiconductor photoanodes, to simultaneously meet these demands. Recently, Fe_2O_3,[5] $BiVO_4$,[6] Ta_3N_5,[7] GaP,[8] GaN/InGaN [9] and Si [10] have been intensively studied as photoanodes. Among these materials, Si is a low cost and abundantly available photoabsorber material, with an energy band-gap of 1.12 eV, which has advantages such as high carrier mobility and absorption of a substantial portion of sunlight.[4, 11] Si, however, is highly prone to photocorrosion.[10a, 12] Various surface protection schemes, including the use of TiO_2 and NiO_x, have been developed to improve the stability of Si-based photoanodes.[8, 13] The use of wide bandgap and/or thick protection layers, however, severely limits the extraction of photoexcited holes, leading to very low photocurrent density and extremely poor applied bias photon-to-current efficiency (ABPE) in the range of 1-2%.[8, 10a, 12b, 13b, 13d] Recently, by using NiFe-LDH catalyst with Ni/NiO_x as a protection layer, an ABPE of ~4.3% has been demonstrated for Si photoanodes,[14] which however, still lags significantly behind those (~10-15%) for Si-based photocathodes.[10c, 15]

Studies have shown that earth-abundant two-dimensional (2D) transition metal dichalcogenides (TMDC), including MoS_2,[16] WSe_2,[17] $MoSe_2$ [17b, 18] and WS_2,[19a] possess remarkable properties for PEC application. The edge states of monolayer TMDC can provide catalytic sites for H_2 evolution reaction

(HER),[19] and TMDCs have also been employed as photoanodes for oxidation reaction.[16, 17b, 17d, 18, 20] Recent first principles calculations have further revealed that perfect 2D TMDCs are chemically inert,[21] and their excellent stability in acidic electrolyte has also been reported.[22] Due to the van der Waals bonds, high quality interface can be formed when 2D TMDC is deposited on Si surface, which can offer an effective means to passivate the Si surface and minimize surface recombination.[23] To date, however, there have been no reports on the use of 2D TMDCs as a surface protection layer for semiconductor photoanodes. This has been limited, to a large extent, by the lack of controllable synthesis process of 2D TMDCs. The commonly used exfoliation process is not suited to produce uniform TMDCs with controlled thickness and high-quality interface on a large area wafer.[24a, 24b] Alternatively, the growth/synthesis of 2D TMDCs using bottom-up approaches such as chemical vapor deposition (CVD) and molecular beam epitaxy (MBE) have been intensively studied.[24] The latter method, which utilizes ultrahigh vacuum (UHV) environment, is highly promising to produce high purity and controllable film thickness.[24a, 24b, 25]

Herein, we have investigated the MBE growth of large area $MoSe_2$ film on p^+-n Si substrate and have further studied the PEC performance of Si photoanode with $MoSe_2$ protection layers of varying thicknesses. It is observed that the incorporation an ultrathin (~3 nm) epitaxial $MoSe_2$ can significantly enhance the performance and stability of p^+-n Si photoanode. The $MoSe_2$/p^+-n Si photoanode produces a nearly light-limited current density of ~30 mA/cm^2 in 1M HBr under AM 1.5G one sun illumination, with a current-onset potential of 0.3 V *vs* RHE. The ABPE reaches up to 13.8%, compared to the negligible ABPE values (< 0.1%) of bare Si photoanode. Moreover, nearly 100% hole injection efficiency is achieved under a relatively low voltage of < 0.6 V *vs* RHE. The chronovoltammetry analysis for the photoanode shows a stable voltage of ~0.38 V *vs* RHE for ~14 hrs at ~2 mA/cm^2. The effect of $MoSe_2$ layer thickness on the PEC performance is also investigated. This work shows the extraordinary potential

of 2D TMDC in PEC application and promises a viable approach for achieving high efficiency Si-based photoanodes.

Schematically shown in Figure 1a, $MoSe_2$ films were grown on p^+-n Si substrate using a Veeco GENxplor MBE system. The fabrication of p^+-n Si wafer is described in Supp. Info. Section 1. As described in Experimental Section, the MBE growth of $MoSe_2$ thin film results in 2H structure,[24b] which is schematically shown in **Figure 1a**. The energy band diagram of the $MoSe_2$/p^+-n Si photoelectrode is illustrated in **Figure 1b**. Photoexcited holes can tunnel through the thin $MoSe_2$ protection layer to participate in oxidation reaction, while photoexcited electrons from Si migrate towards the counter electrode to participate in H_2 evolution reaction. The $MoSe_2$ layer also suppresses surface recombination.[23b] It is seen that the thickness of $MoSe_2$ is critical: it needs to be optimally designed and synthesized to protect the Si surface against photocorrosion and oxidation without compromising the hole transport and extraction.

Properties of $MoSe_2$ grown on Si wafer by MBE are characterized using X-ray photoelectron spectroscopy (XPS), atomic force microscopy (AFM), and micro-Raman spectroscopy. We have first analyzed the composition of $MoSe_2$ layers by using XPS measurement (Thermo Scientific K-Alpha XPS system with a monochromatic Al Kα source (hν=1486.6 eV)). The binding energy of carbon (284.58 eV) was used as a reference peak position for the measurements. **Figure 2a** shows two peaks located at 229.2 and 232.4 eV which originated from Mo $3d_{5/2}$ and Mo $3d_{3/2}$ orbitals, respectively, confirming the existence of Mo^{4+}.[26] Shown in **Figure 2b**, a single doublet of Se $3d_{5/2}$ at 54.9 eV and Se $3d_{3/2}$ at 55.6 eV can be observed, corresponding to the oxidation state of -2 for Se.[24b, 24e, 26] These results confirm the formation of $MoSe_2$ on the Si wafer. Micro-Raman spectroscopy was carried out using a 514 nm argon ion laser as the excitation source. Illustrated in **Figure 2c**, emission peaks at 163.02, 235.67, 281.89 and 346.18 cm^{-1} have been identified, which correspond to E_{1g}, A_{1g}, $E_{2g}{}^1$ and $A_{2u}{}^2$ modes, respectively. The most prominent

peaks are A_{1g} and E_{2g}^1 modes, which are related to the out-of-plane vibration and in-plane vibration, respectively. These Raman modes, unique to 2H-$MoSe_2$, have been observed in previous reports and suggest the formation of 2H-phase $MoSe_2$ on Si wafer.[27] Shown in **Figure 2d** is the AFM image of $MoSe_2$ film (~3 nm thick) grown on Si (also see Supp. Info. Section 3).

We have subsequently investigated the PEC performance of $MoSe_2/p^+$-*n* Si photoanode. The linear scan voltammogram (LSV) of $MoSe_2/p^+$-*n* Si photoanodes with various $MoSe_2$ thicknesses is shown in **Figure 3a** under both dark and illumination conditions. Further details of the LSV for p^+-*n* Si photoanode with and without any $MoSe_2$ coverage are shown in Supp. Info. Section 4. It is observed that the p^+-*n* Si photoanode exhibit negligible photocurrent, which is directly related to the rapid surface oxidation of unprotected Si surface.[28] Superior performance was achieved for $MoSe_2/p^+$-*n* Si photoanodes with ~3 nm $MoSe_2$. Shown in **Figure 3a**, the current-onset potential is ~0.3 V *vs* RHE, with a nearly light-limited current density ~30 mA/cm^2 measured at ~0.8 V *vs* RHE (see Supp. Info. Section 5). The measurement of light-limited current density also suggests that the thin $MoSe_2$ layer can effectively passivate the Si surface to minimize surface recombination. The achievement of high photocurrent density for a photoanode under relatively low bias voltage is essentially required to realize unassisted solar H_2 generation when paired with a high-performance photocathode for PEC tandem system. With increasing $MoSe_2$ thickness to ~5 nm, the photocurrent density is reduced to ~27 mA/cm^2, due to the less efficient tunneling of photo-excited holes from Si to electrolyte. It is worth mentioning that the reduction of photocurrent density may be partly related to the increased absorption of $MoSe_2$ protection layer due to the slightly larger thickness. Previous studies have shown that the hole tunneling through the protection layer is extremely sensitive to the layer thickness.[8b] In this study, since the surface roughness is relatively large (~ 1-2 nm) for $MoSe_2$ layers, we observed a relatively small difference in the photocurrent density by increasing the thicknesses from 3 nm to 5 nm. Also for these reasons, it is observed that decreasing the

$MoSe_2$ thickness to ~1 nm leads to negligible photocurrent density, due to the uneven surface coverage and the resulting oxidation of the Si surface. With further increasing the $MoSe_2$ thickness to ~10 nm, both the photocurrent density and current-onset potential become significantly worse, due to the suppressed tunneling for photo-generated holes. In these studies, the underlying Si wafers are identical and are contacted from the backside. Therefore, the drastically different PEC characteristics are directly related to the thicknesses of $MoSe_2$ protection layer, which provides unambiguous evidence that an optimum thickness of epitaxial $MoSe_2$ can protect the semiconductor photoanode without compromising the extraction of photo-generated holes. Through detailed studies on the $MoSe_2$ growth temperature and *in situ* annealing conditions (see Supp. Info. Section 2), it was identified that the best performing $MoSe_2/p^+$-*n* Si photoanodes could be achieved for $MoSe_2$ thickness ~3 nm and growth temperature in the range of 200 to 400 °C.

The ABPE of the photoanode was derived using the **Equation (1)**,

$$\eta(\%) = \frac{J(E^0_{rev} - V_{RHE})}{P_{in}} \times 100 \quad (1)$$

where J is the photocurrent density, E^0_{rev} is the standard electrode oxidation potential for Br^-, V_{RHE} is the applied bias *vs* RHE, and P_{in} is the power of the incident light (*i.e.* 100 mW/cm^2). Variations of the ABPE *vs* applied bias are shown in **Figure 3b** for $MoSe_2/p^+$-*n* Si photoanodes with $MoSe_2$ thicknesses varying from 1 to 10 nm. It is seen that a maximum ABPE of 13.8% is achieved at ~0.5 V *vs* RHE for $MoSe_2/p^+$-*n* Si photoanodes with $MoSe_2$ thickness ~3 nm. The maximum ABPE decreases to ~12% and 2% with increasing $MoSe_2$ thickness to 5 and 10 nm, respectively, and to negligible values for $MoSe_2$ thicknesses of 1 nm or less. The reported ABPE of 13.8% is significantly higher than previously reported TMDC-based photoanode in polyhalide-based redox systems and hole scavenger solutions.[17b-d, 18, 29] However, the cost of using HBr for solar-to-hydrogen production needs to be analyzed, compared to water splitting.[30] The incident-photon-to-current-efficiency (IPCE) of $MoSe_2/p^+$-*n* Si photoanode with $MoSe_2$

thickness ~3 nm was further measured. The measurement was conducted at 1 V *vs* RHE in 1M HBr in a three-electrode system. The IPCE was calculated using the **Equation (2)**,

$$IPCE\ (\%) = {}^{(1240\ \times I)}\Big/_{(\lambda\ \times P_{in})}\ \times 100 \qquad (2)$$

where I is photocurrent density (mA/cm^2), λ is the incident light wavelength (nm) and P_{in} is the power density (mW/cm^2) of the incident illumination. Shown in **Figure 3c**, the maximum IPCE is above 70%.

We have further studied the open circuit potential (OCP) of $MoSe_2$/p^+-n Si photoanodes, which was measured *vs* RHE under chopped light illumination. A negative shift of the OCP was measured under light illumination, which is characteristic of photoanodes. The OCP (E_{ocp} *vs* RHE) of p^+-n Si and $MoSe_2$/p^+-n Si with $MoSe_2$ thickness ~3 nm is shown in **Figure 4a**. The p^+-n Si photoanode (dotted blue curve) exhibits a dark potential ~0.3 V and an illuminated potential ~0 V, with a change in OCP ~0.3 V. The change in OCP under dark and illumination conditions is less than the photovoltage ~0.53 V for a typical p^+-n Si junction, which is due to the change of potential drop across the Helmholtz layer at the Si/electrolyte interface. E_{ocp} of the $MoSe_2$/p^+-n Si photoanode (solid red curve) is ~0.3 V and 0.8 V *vs* RHE under illumination and dark conditions, respectively. The potential difference under light and dark conditions is ~0.5 V, which is nearly identical to the flat-band potential (V_{fb}) derived from the Mott-Schottky measurements (see Supp. Info. Section 6). Moreover, the light-induced OCP shift (~0.5 V) for $MoSe_2$/p^+-n Si photoanode is reasonably close to the open circuit voltage expected from the p^+-n Si junction. The negligible voltage loss further confirms that the thin (~3 nm) $MoSe_2$ layer can effectively protect the Si surface from oxidation in acidic solution and that photoexcited holes can tunnel efficiently through the $MoSe_2$ layer. Chronovoltammetry experiments were further performed to test the stability of $MoSe_2$/p^+-n Si photoanode at photocurrent density of ~2 mA/cm^2 under AM 1.5G one sun illumination. Shown in **Figure 4b**, the voltage stays nearly constant at ~0.38 V vs RHE, and there is no any apparent degradation under continuous illumination for ~14 hrs. The chronoamperometry experiment (Supp. Info. Section 7)

also showed stable photocurrent density of ~26 mA/cm^2 for 1 hr at 0.6 V vs RHE and subsequent XPS measurements on that sample showed Mo:Se ratio of 1:2.

The underlying mechanisms for the dramatically improved performance of Si-based photoanodes are described. The use of a $MoSe_2$ protection layer allows for the efficient tunneling of photoexcited holes from p^+-n Si to electrolyte through the $MoSe_2$ barrier, compared to the previously reported wide bandgap, e.g. TiO_2 protection layer.[8, 31] This is evidenced by the very large hole injection efficiency (>80%) even at a relatively low potential (~0.5 V *vs* RHE) (see Supp. Info. Section 8). Moreover, the $MoSe_2$ layer is sufficiently thin (~3 nm) to allow for most of the incident light to pass through, thereby leading to a nearly light-limited current density. For a perfect $MoSe_2$ sheet, there are no dangling bonds and surface states, since the lone pair of electrons on chalcogen (Se) atom terminate on the surface.[23a] Recent first principles calculations have further shown that a perfect $MoSe_2$ sheet is intrinsically chemically inert and can effectively protect against oxidation [21, 23a] and photocorrosion,[23a] which explains the dramatically improved performance and stability, compared to a bare Si photoanode. It is also worthwhile mentioning that the enhanced performance is not likely due to the catalytic property of $MoSe_2$, since the $MoSe_2$ layer showed no activity under dark condition (see Figure S4 and Figure 3a) and the 1 nm thickness sample (in Figure 3a) showed very poor light scan. To further improve the device stability, it is essential to eliminate, or minimize the presence of Se vacancy and related defects, which are known to significantly enhance the oxidation effect.[21, 32]

In conclusion, we have demonstrated that the integration of few-layer $MoSe_2$ can protect the surface of an otherwise unstable Si photoelectrode in corrosive environment, while allowing for efficient electron/hole tunneling between Si photoanode and solution. The $MoSe_2$/p^+-n Si photoanode exhibit remarkable PEC performance, including an excellent current-onset potential of 0.3 V *vs* RHE, a light-limited current photocurrent density of ~30 mA/cm^2 under AM1.5G one sun illumination, an ABPE of

13.8%, and relatively high stability in acidic solution. For future work, it would be important to investigate and optimize the $MoSe_2$/Si heterointerface, to engineer the surface properties of $MoSe_2$, and to couple with suitable water oxidation co-catalysts, which will further improve the current-onset potential and enhance the photoanode performance and stability in PEC water splitting. These studies will contribute to the development of low cost, high efficiency, and highly stable Si-based photoelectrodes for solar H_2 production.

Experimental section

Fabrication of p^+-n Si: Double side polished n-type Si(100) wafers (WRS Materials, thickness: 254 – 304 μm; resistivity: 1 - 10 Ω·cm) were spin-coated with liquid boron dopant precursor (Futurrex, Inc.) on one side to form the p^+-Si emitter and liquid phosphorus dopant precursor (Futurrex, Inc.) on the other side to form the n^+-Si back field layer. Subsequently, the thermal diffusion process was conducted at 950 ^oC for 240 min under argon gas flow in a furnace. The residue of the precursor was removed in buffered oxide etch solution. To measure the efficiency of the solar cells, metal contacts were made on *n*-side and *p*-side by depositing Ti/Au and Ni/Au respectively using e-beam evaporator. Shown in Figure S1, J_{sc} of the device is ~31 mA/cm^2, V_{oc} is ~0.52 V, and the energy conversion efficiency is ~11%.

PEC measurements: The PEC reaction was conducted in 1 mol/L HBr solution using a potentiostat (Gamry Instruments, Interface 1000) with $MoSe_2$/p^+-n Si, silver chloride electrode (Ag/AgCl), and Pt wire as the working, reference, and counter electrode, respectively. The working electrode was prepared by cleaving the $MoSe_2$/p^+-n Si wafer into area sizes of 0.2 – 1 cm^2. A Ga−In eutectic (Sigma Aldrich) alloy was deposited on the backside of the Si wafer to form ohmic contact, which was subsequently connected to a Cu wire using silver paste. The entire sample except the front surface was covered by insulating epoxy and placed on a glass slide. A solar simulator (Newport Oriel) with an AM1.5 G filter was used as the

light source, and the light intensity was calibrated to be 100 mW/cm^2 for all subsequent experiments. The conversion of the Ag/AgCl reference potential to RHE is calculated using the **Equation (3)**,

$$E_{(RHE)} = E_{Ag/AgCl} + E^{o}_{Ag/AgCl} + 0.059 \times pH \quad (3)$$

where $\boldsymbol{E^{o}_{Ag/AgCl}}$ is 0.197 V, and pH of the electrolyte is nearly zero.

MBE growth of $MoSe_2$: During the growth process, molybdenum (Mo) was thermally evaporated using an e-beam evaporator (Telemark Inc.) retrofitted in the MBE reaction chamber. We have developed a two-step MBE growth process for $MoSe_2$ thin film. In the first step, the substrate was heated to temperatures in the range of 200-450 ^{o}C, and Mo molecular beam was introduced under Se-rich conditions (Se beam equivalent pressure (BEP) of 3.5 × 10^{-7} torr) for 18-180 minutes, with a deposition rate ~0.01 Å/s for $MoSe_2$. The resulting $MoSe_2$ thicknesses vary between 1nm and 10 nm. In the second step an *in situ* thermal annealing was performed under Se flux for 10 mins in the temperature range of 200-650 ^{o}C (see Supp. Info. Section 2).

Supporting Information

Supporting Information is available from the Wiley Online Library or from the author.

Acknowledgements

This work is being supported by the Emissions Reduction Alberta (ERA).

Competing financial interests. The authors declare no competing financial interests.

References

[1] S. Chu, A. Majumdar, *Nature* **2012,** 488, (7411), 294-303.

[2] a) M. G. Walter, E. L. Warren, J. R. McKone, S. W. Boettcher, Q. X. Mi, E. A. Santori, N. S. Lewis, *Chem. Rev.* **2010,** 110, (11), 6446-6473; b) Y. Hou, X. Zhuang, X. Feng, *Small Methods* **2017,** 1, (6), 1700090; c) B. Parkinson, J. Turner, *Photoelectrochemical Water Splitting: Materials, Processes and Architectures*, Chapter-1, The Royal Society of Chemistry **2013**, 1-18; d) M. Gratzel, *Nature* **2001,** 414, (6861), 338-344.

[3] a) J. A. Turner, *Science* **2004,** 305, (5686), 972-974; b) N. S. Lewis, D. G. Nocera, *Proc. Natl. Acad. Sci. U S A* **2006,** 103, (43), 15729-35.

[4] S. Hu, C. X. Xiang, S. Haussener, A. D. Berger, N. S. Lewis, *Energ. Environ. Sci.* **2013,** 6, (10), 2984-2993.

[5] a) K. Sivula, F. Le Formal, M. Gratzel, *ChemSusChem* **2011,** 4, (4), 432-49; b) S. Shen, S. A. Lindley, X. Chen, J. Z. Zhang, *Energ. Environ. Sci.* **2016,** 9, (9), 2744-2775.

[6] a) Y. Park, K. J. McDonald, K.-S. Choi, *Chem. Soc. Rev.* **2013,** 42, (6), 2321-2337; b) I. D. Sharp, J. K. Cooper, F. M. Toma, R. Buonsanti, *ACS Energ. Lett.* **2017,** 2, (1), 139-150.

[7] a) M. Li, W. Luo, D. Cao, X. Zhao, Z. Li, T. Yu, Z. Zou, *Angew. Chem. Int. Ed.* **2013,** 52, (42), 11016-11020; b) M. Zhong, T. Hisatomi, Y. Sasaki, S. Suzuki, K. Teshima, M. Nakabayashi, N. Shibata, H. Nishiyama, M. Katayama, T. Yamada, K. Domen, *Angew. Chem. Int. Ed.* **2017,** 56, (17), 4739-4743.

[8] a) S. Hu, M. R. Shaner, J. A. Beardslee, M. Lichterman, B. S. Brunschwig, N. S. Lewis, *Science* **2014,** 344, (6187), 1005-1009; b) M. T. McDowell, M. F. Lichterman, A. I. Carim, R. Liu, S. Hu, B. S. Brunschwig, N. S. Lewis, *ACS Appl. Mater. Interfaces* **2015**, 7, (28), 15189-99.

[9] a) S. Fan, I. Shih, Z. Mi, *Adv. Energ. Mater.* **2016**, 1600952-n/a ; b) B. AlOtaibi, S. Fan, S. Vanka, M. G. Kibria, Z. Mi, *Nano Lett.* **2015,** 15, (10), 6821-8.

[10] a) B. Mei, B. Seger, T. Pedersen, M. Malizia, O. Hansen, I. Chorkendorff, P. C. K. Vesborg, *J. Phys. Chem. Lett.* **2014,** 5, (11), 1948-1952; b) X. H. Zhou, R. Liu, K. Sun, K. M. Papadantonakis, B. S. Brunschwig, N. S. Lewis, *Energ. Environ. Sci.* **2016,** 9, (3), 892-897; c) H. P. Wang, K. Sun, S. Y. Noh, A. Kargar, M. L. Tsai, M. Y. Huang, D. L. Wang, J. H. He, *Nano Lett.* **2015,** 15, (5), 2817-2824.

[11] K. Sun, S. H. Shen, Y. Q. Liang, P. E. Burrows, S. S. Mao, D. L. Wang, *Chem. Rev.* **2014,** 114, (17), 8662-8719.

[12] a) H. Gerischer, *Faraday Discussions of the Chemical Society* **1980,** 70, (0), 137-151; b) M. J. Kenney, M. Gong, Y. Li, J. Z. Wu, J. Feng, M. Lanza, H. Dai, *Science* **2013,** 342, (6160), 836-840.

[13] a) Y. W. Chen, J. D. Prange, S. Duhnen, Y. Park, M. Gunji, C. E. D. Chidsey, P. C. McIntyre, *Nat. Mater.* **2011,** 10, (7), 539-544; b) X. H. Zhou, R. Liu, K. Sun, D. Friedrich, M. T. McDowell, F. Yang, S. T. Omelchenko, F. H. Saadi, A. C. Nielander, S. Yalamanchili, K. M. Papadantonakis, B. S. Brunschwig, N. S. Lewis, *Energ. Environ. Sci.* **2015,** 8, (9), 2644-2649; c) G. Xu, Z. Xu, Z. Shi, L. Pei, S. Yan, Z. Gu, Z. Zou, *ChemSusChem* **2017,** 10, (14), 2897-2903; d) K. Sun, M. T. McDowell, A. C. Nielander, S. Hu, M. R. Shaner, F. Yang, B. S. Brunschwig, N. S. Lewis, *J. Phys. Chem. Lett.* **2015,** 6, (4), 592-8.

[14] B. Guo, A. Batool, G. Xie, R. Boddula, L. Tian, S. U. Jan, J. R. Gong, *Nano Lett.*, **2018**, 18, (2), 1516-1521.

[15] R. Fan, W. Dong, L. Fang, F. Zheng, M. Shen, *J. Mater. Chem. A* **2017**, 5, 18744-18751.

[16] a) X. Xu, G. Zhou, X. Dong, J. Hu, *ACS Sustain. Chem. Eng.* **2017,** 5, (5), 3829-3836; b) F. M. Pesci, M. S. Sokolikova, C. Grotta, P. C. Sherrell, F. Reale, K. Sharda, N. Ni, P. Palczynski, C. Mattevi, *ACS Catal.* **2017,** 7, (8), 4990-4998.

[17] a) J. R. McKone, A. P. Pieterick, H. B. Gray, N. S. Lewis, *J. Am. Chem. Soc.* **2013,** 135, (1), 223-31; b) G. Kline, K. Kam, D. Canfield, B. A. Parkinson, *Sol. Energ. Mater.* **1981,** 4, (3), 301-308; c) H. J.

Lewerenz, A. Heller, F. J. DiSalvo, *J. Am. Chem. Soc.* **1980,** 102, (6), 1877-1880; d) R. Tenne, A. Wold, *Appl. Phys. Lett.* **1985,** 47, (7), 707-709.

[18] L. P. Bicelli, G. Razzini, *Surface Technology* **1982,** 16, (1), 37-47.

[19] a) X. Yu, M. S. Prevot, N. Guijarro, K. Sivula, *Nat. Commun.* **2015,** 6, 7596; b) Y. Ouyang, C. Ling, Q. Chen, Z. Wang, L. Shi, J. Wang, *Chem. Mater.* **2016,** 28, (12), 4390-4396; c) A. K. Singh, K. Mathew, H. L. Zhuang, R. G. Hennig, *J. Phys. Chem. Lett.* **2015,** 6, (6), 1087-98;

[20] R. Bourezg, G. Couturier, J. Salardenne, F. Lévy, *Phys. Rev. B* **1992,** 46, (23), 15404-15410.

[21] H. Liu, N. Han, J. Zhao, *RSC Adv.* **2015,** 5, (23), 17572-17581.

[22] L. A. King, T. R. Hellstern, J. Park, R. Sinclair, T. F. Jaramillo, *ACS Appl. Mater. Interfaces* **2017,** 9, (42), 36792-36798.

[23] a) M. Chhowalla, H. S. Shin, G. Eda, L. J. Li, K. P. Loh, H. Zhang, *Nat. Chem.* **2013,** 5, (4), 263-75; b) N. Balis, E. Stratakis, E. Kymakis, *Mater. Today* **2016,** 19, (10), 580-594.

[24] a) E. Xenogiannopoulou, P. Tsipas, K. E. Aretouli, D. Tsoutsou, S. A. Giamini, C. Bazioti, G. P. Dimitrakopulos, P. Komninou, S. Brems, C. Huyghebaert, I. P. Radu, A. Dimoulas, *Nanoscale* **2015,** 7, (17), 7896-905; b) Y. H. Choi, D. H. Lim, J. H. Jeong, D. Park, K. S. Jeong, M. Kim, A. Song, H. S. Chung, K. B. Chung, Y. Yi, M. H. Cho, *ACS Appl. Mater. Interfaces* **2017**; c) Y.-H. Chang, W. Zhang, Y. Zhu, Y. Han, J. Pu, J.-K. Chang, W.-T. Hsu, J.-K. Huang, C.-L. Hsu, M.-H. Chiu, T. Takenobu, H. Li, C.-I. Wu, W.-H. Chang, A. T. S. Wee, L.-J. Li, *ACS Nano* **2014,** 8, (8), 8582-8590; d) X. Lu, M. I. Utama, J. Lin, X. Gong, J. Zhang, Y. Zhao, S. T. Pantelides, J. Wang, Z. Dong, Z. Liu, W. Zhou, Q. Xiong, *Nano Lett.* **2014,** 14, (5), 2419-25; e) F. S. Ohuchi, B. A. Parkinson, K. Ueno, A. Koma, *J. Appl. Phys.* **1990,** 68, (5), 2168-2175.

[25] D. Tsoutsou, K. E. Aretouli, P. Tsipas, J. Marquez-Velasco, E. Xenogiannopoulou, N. Kelaidis, S. Aminalragia Giamini, A. Dimoulas, *ACS Appl. Mater. Interfaces* **2016,** 8, (3), 1836-41.

[26] Y. Zhao, H. Lee, W. Choi, W. Fei, C. J. Lee, *RSC Adv.* **2017,** 7, (45), 27969-27973.

[27] a) C. Jung, S. M. Kim, H. Moon, G. Han, J. Kwon, Y. K. Hong, I. Omkaram, Y. Yoon, S. Kim, J. Park, *Sci. Rep.* **2015,** 5, 15313; b) M. I. Utama, X. Lu, D. Zhan, S. T. Ha, Y. Yuan, Z. Shen, Q. Xiong, *Nanoscale* **2014,** 6, (21), 12376-82; c) D. Nam, J. U. Lee, H. Cheong, *Sci. Rep.* **2015,** 5, 17113; d) P. Soubelet, A. E. Bruchhausen, A. Fainstein, K. Nogajewski, C. Faugeras, *Phys. Rev. B* **2016,** 93, (15).

[28] A. Q. Contractor, J. O. M. Bockris, *Electrochim. Acta* **1984,** 29, (10), 1427-1434.

[29] a) J. R. McKone, R. A. Potash, F. J. DiSalvo, H. D. Abruna, *Phys. Chem. Chem. Phys.* **2015,** 17, (21), 13984-91; b) L. A. King, W. Zhao, M. Chhowalla, D. J. Riley, G. Eda, *J. Mater. Chem. A* **2013,** 1, (31), 8935.

[30] B. Mei, G. Mul, B. Seger, *Adv. Sus. Sys.* **2017**, 1, (1-2), 1600035-n/a.

[31] A. G. Scheuermann, J. P. Lawrence, K. W. Kemp, T. Ito, A. Walsh, C. E. Chidsey, P. K. Hurley, P. C. McIntyre, *Nat. Mater.* **2016,** 15, (1), 99-105.

[32] J. Gao, B. Li, J. Tan, P. Chow, T. M. Lu, N. Koratkar, *ACS Nano* **2016,** 10, (2), 2628-35.

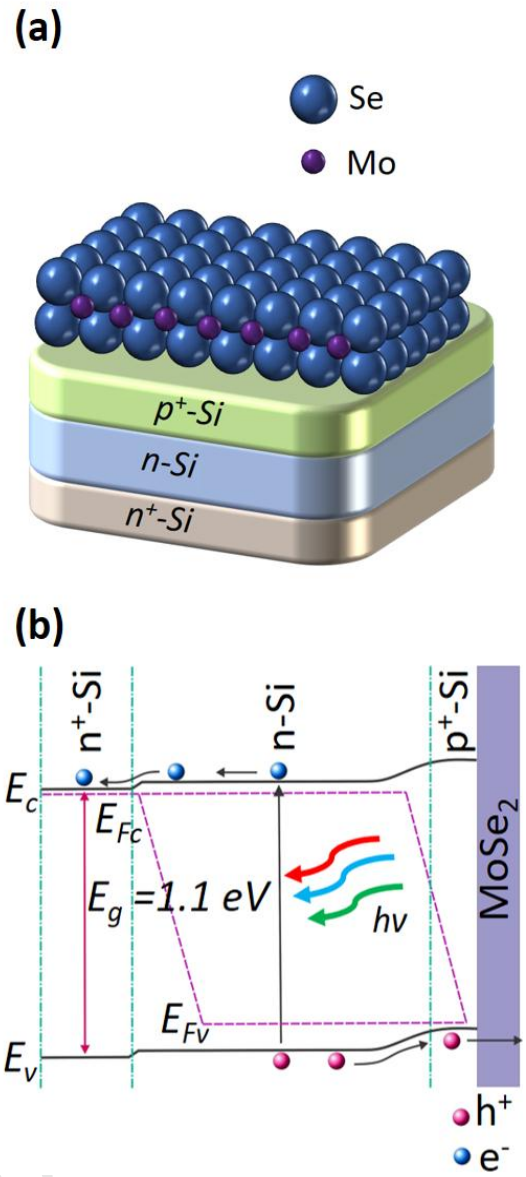

Figure 1. (a) Schematic illustration of p^+-*n* Si photoanode protected by few-layer 2H $MoSe_2$. Dark blue and purple colored atoms denote Se, and Mo, respectively. (b) Schematic of the energy band diagram of $MoSe_2$ /p^+-*n* Si photoanode under AM1.5G light illumination.

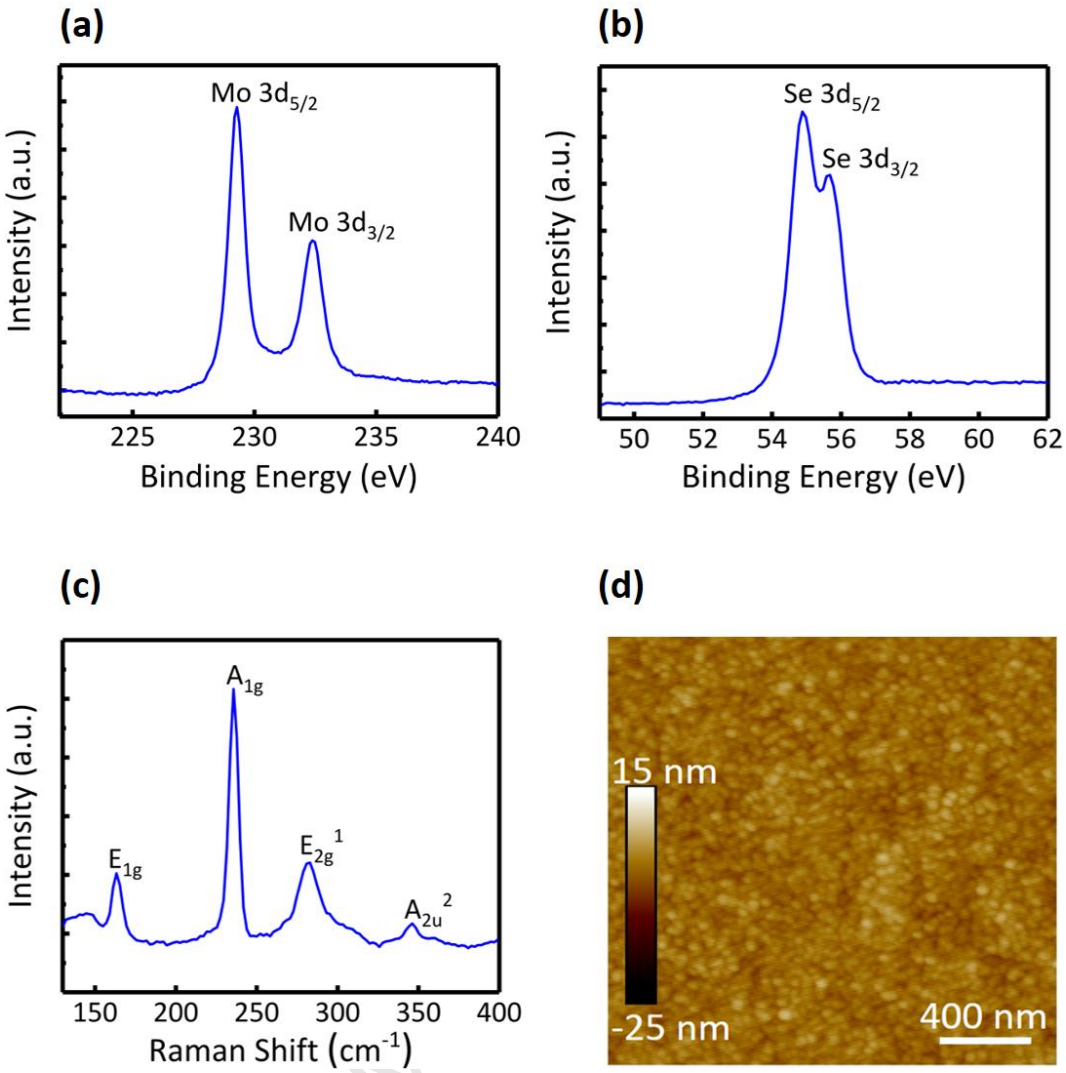

Figure 2. Structural characterization of few-layer $MoSe_2$ grown on Si substrate. XPS measurements show (a) two peaks at 229.2 and 232.4 eV corresponding to Mo^{4+} and (b) doublet of 54.9 and 55.6 eV corresponding to Se^{2-} for $MoSe_2$ film. (c) Raman spectra for $MoSe_2$ film showing E_{1g}, A_{1g}, E_{2g}^1 and A_{2u}^2 modes at 163.02, 235.67, 281.89 and 346.18 cm^{-1}, respectively. (d) AFM image of $MoSe_2$ surface on Si wafer; scale bar 400 nm. The thickness of $MoSe_2$ layer is ~ 3nm.

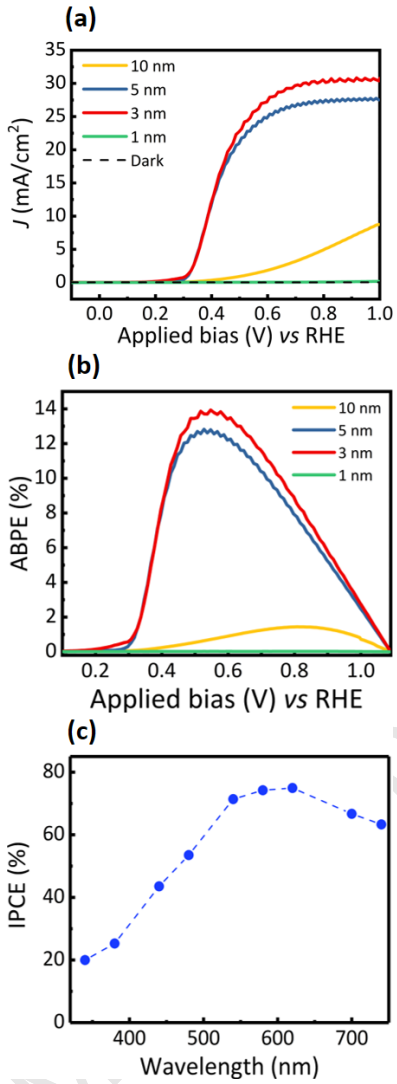

Figure 3. PEC performance characterization of $MoSe_2/p^+$-*n* Si photoanode. (a) *J*-*V* characteristics of $MoSe_2/p^+$-*n* Si photoanode with $MoSe_2$ thicknesses of 1nm (green curve), 3 nm (red curve), 5 nm (blue curve) and 10 nm (yellow curve) under AM1.5G one sun illumination (100 mW/cm^2) and dark condition (black dashed curve) in 1M HBr. (b) ABPE measurement for $MoSe_2/p^+$-*n* Si photoanode with different $MoSe_2$ thicknesses. The highest ABPE of 13.8% was measured for Si photoanode with 3 nm $MoSe_2$ protection layer at ~0.5 V *vs* RHE. (c) IPCE of $MoSe_2/p^+$-*n* Si photoanode under AM1.5G one sun illumination (100 mW/cm^2) in 1 M HBr. The peak value is ~75% at 620 nm.

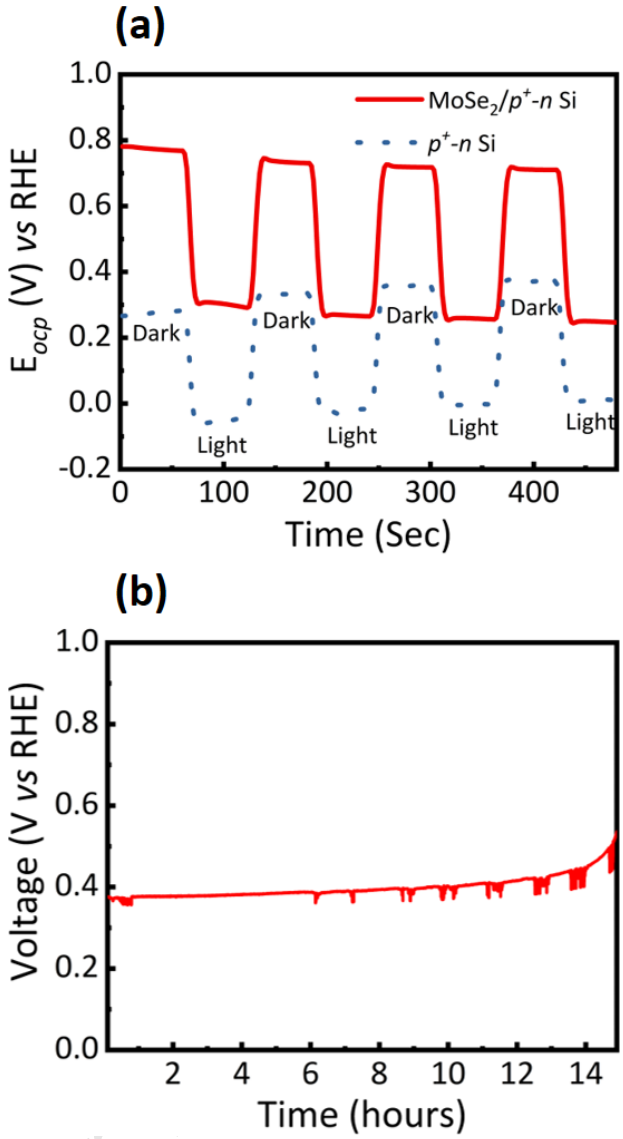

Figure 4. OCP and Stability measurements of $MoSe_2/p^+$-*n* Si photoanode. (a) OCP *vs* RHE under chopped light illumination. Red curve shows OCP for $MoSe_2/p^+$-*n* Si photoanode, and dotted blue curve is OCP for p^+-*n* Si without $MoSe_2$. (b) Stability of $MoSe_2/p^+$-*n* Si photoanode. Chronopotentiometry graph shows stable voltage (*vs* RHE) ~0.38 V for ~14 hrs at ~2 mA/cm^2 under AM 1.5G one sun illumination in 1 M HBr.

The incorporation few-layer (~3 nm) epitaxial $MoSe_2$ can significantly enhance the performance and stability of Si photoanode. The resulting $MoSe_2/p^+$-*n* Si photoanode produces a light-limited current density of 30 mA/cm^2 in 1M HBr under AM 1.5G one sun illumination, with a current-onset potential of 0.3 V *vs* reversible hydrogen electrode (RHE). The applied bias photon-to-current efficiency reaches 13.8% at 0.5 V *vs.* RHE.

Keywords: transitional metal dichalcogenide, two-dimensional material, water splitting, photoelectrode, hydrogen, solar cell

*Srinivas Vanka, Yongjie Wang, Pegah Ghamari, Sheng Chu, Ayush Pandey, Pallab Bhattacharya, Ishiang Shih, and Zetian Mi**

A High Efficiency Si Photoanode Protected by Few-Layer $MoSe_2$